Transient Fluorescence Behavior of Poly(*N*-vinylcarbazole) in Solution. 1. Multiexponential Fluorescence Patterns: Relevancy of a Rate Constant Formalism

Harald F. Kauffmann,* Wolf-Dieter Weixelbaumer, Josef Buerbaumer, Anne-Marie Schmoltner,† and Oskar F. Olaj

Institute of Physical Chemistry, University of Vienna, A-1090 Vienna, Austria.
Received February 16, 1984

ABSTRACT: The transient intrachain fluorescence behavior of cationically prepared poly(*N*-vinylcarbazole) (p-N-VCz), 5×10^{-5} M (unit mol) in benzene solution, was studied by means of conventional time-resolved single-photon-counting. The curves were collected at the emission wavelengths λ_{em} = 460, 370, and 348 nm, and their molecular response profiles fitted to multiexponential functional forms by least-squares iterative reconvolution. The novel result of this analysis concerns the transient profile of the low-energy "sandwich" excimer E_2, which exhibits a significant *triple*-exponential behavior, consisting of a *biexponential* growth term—with apparent rise times $T_2 \cong 0.4$ ns and $T_3 \cong 3$ ns—and of a monoexponential decay term, with $T_4 \cong 35$ ns. Similar values of time constants T_2, T_3, and T_4, in addition to $T_5 \cong 10$ ns, were found from the four-exponential fit of the transient decay curves at λ_{em} = 370 nm and at λ_{em} = 348 nm. While the spectral region, centered at the emission wavelength λ_{em} = 370 nm, represents the high-energy domain of quasi "preformed" excimers and traps, a considerable part of the peak shoulder near 348 nm corresponds to the 0–0 transition of the excited monomeric carbazole unit, M*, which must be generally considered to be an inherent intrachain component in electronically excited dilute p-N-VCz systems. Neglecting—as a rudimentary approach—the nonexponential complications with respect to energy migration and nondiffusive segmental dynamics which proceed in the nonresolvable picosecond transient regime, an attempt is made to interpret the long-time behavior of both the high-energy and the low-energy transient curves in terms of a rate constant formalism. The population of E_2 is treated in a coupled scheme of four species M*, E_2, Tr_1, and Tr_2 in which two kinetically distinct picosecond traps Tr_1 and Tr_2 act as excited-state intermediates in a series of reversible and irreversible energy cascading pathways. Analytical solutions for the respective time profiles are given and the validity of the scheme is tested with plausible trial data in preliminary computational evaluations.

I. Introduction

Recently, many reports concerning time-resolved fluorescence studies on synthetic aromatic homopolymers and copolymers in solution have been published. In particular, attention has been focused on the time-dependent fluorescence behavior of polystyrene,[1-3] poly(1-vinylnaphthalene) (p-1-VN),[1,4-6] and poly(2-vinylnaphthalene) (p-2-VN),[7-9] and on the transient emission characteristics of copolymers of 1-vinylnaphthalene (1-VN) and methyl methacrylate (MMA)[10-12], of 1-VN and methyl acrylate (MA),[13] and of 2-VN and styrene,[14] as well as of a series of other naphthalene-containing polymers.[5,15-18] For all these polymers the analysis of the relaxation profiles has revealed a lot of complexity and has led to a great deal of discussion with respect to the pathways in excited-state dynamics of polychromophoric macromolecular systems in dilute solution. It is commonly observed in these systems that (1) the monomer fluorescence data of randomly excited chromophores can be numerically resolved by the sum of three exponentials and (2) the excimer emission profiles seem to require fit functions consisting of a linear combination of more than two exponentials. These results are indicative of the fact that the local proximity of identical chromophores attached to the C–C backbone of the chain cannot be treated in analogy to the diffusive, collisional self-quenching process in concentrated solutions—according to the small-molecule limit in the kinetic schemes of Birks[19,20] and Klöpffer.[21-23] The invalidity of a dissociative monomer–excimer concept in singlet excited-state kinetics of macromolecules has led to strategies which try to correlate the number of exponentials observed to the number of states interacting in coupled kinetic schemes. Thus, the additional kinetic species was claimed to be a "high-energy" excimer with a partially overlapped sandwich structure of naphthyl rings in the case of p-1-VN[6] and of poly(1-methoxy-4-vinylnaphthalene)[24] and in dimeric model compounds of substituted dinaphthylpropanes.[25] Moreover, an exo excimer and an endo excimer were postulated in the case of bis(1-naphthylmethyl) ether.[26] On the other hand, a rotational isomeric state model of electronically excited conformers[27] was proposed for p-2-VN,[7,8] for bis(2-naphthylethyl ether),[7,8] for the copolymers of 1-VN and MMA,[10-12] and for 1,3-dicarbazolylpropane[28] to account for their complicated transient profiles.

Poly(*N*-vinylcarbazole) (p-N-VCz), however, displays an even more complex behavior in this class of poly(vinylaromatic) systems. Numerous groups of authors[28,29-31] attempted to identify its complex fluorescence decay on the basis of an equilibrium between a low-energy "sandwich-type" excimer E_2 and a "high-energy" excimer E_1,[29] while others,[32,33] from the analysis of stereochemically pure 2,4-di(*N*-carbazolyl)pentanes, which act as dimeric models for a three-skeletal-carbon rotational dyad of isolated, isotactic and syndiotactic segmental sequences in p-N-VCz, more recently hypothesized the additional importance of conformational aspects upon intramolecular excimer formation.[34] Nevertheless, it appears that the fluorescence behavior of low molecular weight bichromophoric model compounds cannot account for the complex morphology. Thus, the rather short delay in the buildup kinetics of the excimer population of E_1[29,35] strongly indicates that energy migration[36,37] may reveal itself as a fast event in the trapping process. In particular, for p-N-VCz it is to be anticipated that electronic, interchromophoric excited-state coupling to "preformed" excimer-forming sites[29,38] is the predominant process while rotational sampling subsequent to monomer excitation takes place on a longer time scale and contributes to a small extent only. Contrary to these observations, the δ-fluorescence response of the low-energy excimer E_2 at the emission wavelength λ_{em} = 470 nm was reported to show a considerably long

† Present address: Department of Chemistry, Berkeley, CA; Fulbright Fellowship 1983–1984.

0024-9297/85/2218-0104$01.50/0

delay in the rising part, with a rise time of approximately 2.5 ns.[39] This characteristic mode of an energy-trapping process on a nanosecond time scale was discussed in terms of a rotational alignment of a third excimer E_3 into the sandwich dimer E_2.

The third excimer E_3 must be discussed within the rather unsharp limits of a phantom state as in fact nothing is known with respect to its configuration and its spectral photon intensity distribution. Only its intermediate role in an energy cascading process has been established as it must act as a precursor of the totally eclipsed conformation of two carbazole moieties in a trans–trans meso dyad of E_2. While it is likely that its energetic position and its time evolution may be comparable with the energetic and kinetic parameters of the high-energy excimer E_1, no valid conclusion can be drawn regarding the shape of the spectral width of its emission band. It seems possible, however, that the fluorescence of E_3 spectrally overlaps with the short-wavelength wing of the emission spectrum of E_2. Thus, for example, the highly intractable data in time-resolved fluorescence analysis of E_2 at the emission wavelength λ_{em} = 420 nm[28] have been satisfactorily explained in terms of a spectral admixture of E_3 to E_2.[40]

Nevertheless, it must be emphasized that the general morphological situation of p-N-VCz in solution contains the inherent complexity of a multiparticle system with a nonuniform distribution of chromophores. This problem has been recently attacked by the Stanford group.[41-43] Moreover, it has been widely established that—according to the different kinetic mechanisms of its formation—p-N-VCz consists of variable ratios of isotactic and syndiotactic segmental sequences.[34,44,45] Thus, it exhibits a considerable conformational multiplicity whereas the perturbative second-order interaction between each type of stereoisomeric sequence should lead to a further degeneracy and, as a result, to a breakdown of the rotational isomeric state model. This can be realistically displayed in a physical model of narrowly spaced energy levels of excimer-forming sites {E}. Due to the electronic excited-state transport subsequent to the monomeric chromophore excitation and because of the consecutive character of electronic energy dissipation, each of the particular conformations of neighbor carbazole units must be considered to be involved in a rather complex series of population and deactivation steps, respectively. Since some of these traps can be assumed to be emissive and energetically comparable, it is the spectral superposition of photons which leads to a further complication, inasmuch as—first of all—it prevents the exact evaluation of relative amplitudes in a transient experiment. It becomes evident from these considerations that the transient excimer and trap fluorescence profiles should yield at least a series of exponentials whereas the number of exponentials actually observed from reconvolution techniques would depend on the finite resolution power of the transient apparatus and the fit routines. Thus, the numerically resolved three-exponential fluorescence decay of p-N-VCz in the high-energy region at λ_{em} = 360 nm[39] and λ_{em} = 370 nm[46] was interpreted in terms of a superposition and a partial interrelation of three excimer states E_1, E_2, and E_3, respectively, among which E_3 was treated as a kinetically distinguishable phantom entity which may reflect the multitude of high-energy excimer states in the short-wavelength region of excimer emission.

In order to reveal the multicomponent contributions of particular conformations, which are spectrally superimposed to both the excimers E_1 and E_2, it is necessary to analyze systematically the time-resolved fluorescence profiles as a function of emission wavelength across the broad spectral range of p-N-VCz emission. Thus, one approach to the inhomogeneity of the p-N-VCz fluorescence should be the collection of a series of experimental fluorescence convolutes at distinct wavelength intervals. Deconvolutions of these curves, generation of artificial profiles with the best fit decay parameters from the experimental data, and finally their normalization would lead to the synthesis of deconvolved time-resolved emission spectra. So far, no study has been reported for p-N-VCz with regard to the analysis of its "decay associated spectra", which were first proposed and developed by Brand et al.[47] As a preliminary result of such a study we want to report in this paper the transient fluorescence curves of cationically prepared p-N-VCz in dilute benzene solution at the emission wavelengths λ_{em} = 348 nm, λ_{em} = 370 nm, and λ_{em} = 460 nm, which correspond to the excited monomer M*, to the maximum emission intensity in the overlap region with E_1, and to the spectrally pure, low-energy excimer E_2, respectively. The first novel aspect we consider in this work concerns the significant triple-exponential fluorescence pattern of E_2 at λ_{em} = 460 nm. A further important point deals with the nonnegligible stationary monomer contribution of fluorescence at λ_{em} = 348 nm. As it will be shown, the decay of the excited monomer can be very satisfactorily fitted to a sum of *four* exponentials. Finally, we intend to show that both fluorescence patterns at λ_{em} = 460 nm and at λ_{em} = 348 nm provide sufficient justification for a semiquantitative treatment of a scheme which takes into account the interconversion between the excited monomer, M*, the low-energy excimer, E_2, and *two* quasi "preformed" picosecond traps, Tr_1 and Tr_2, respectively. In this work we assume a rate constant mechanism and thus approximately disregard the influence of nonexponential energy migration and trapping,[41-43] as well as the contribution of nondiffusive phenomena[48,49] to the rotational sampling processes.[50]

II. Experimental Section

Materials. Preparation. Benzene (Merck, spectrograde, for fluorescence spectroscopy) was used as supplied without further purification.

Dichloromethane (Merck, reagent grade) was distilled from calcium hydride prior to use.

***N*-Vinylcarbazole** monomer (BASF) was repeatedly recrystallized from methanol.

Poly(*N*-vinylcarbazole) (p-N-VCz) was prepared by cationic polymerization of *N*-vinylcarbazole (2.8×10^{-1} M) in the presence of 1:1 trityl chloride/antimony pentachloride (10^{-4} M) initiator in dry dichloromethane at −40 °C. p-N-VCz samples were purified by repeated precipitation from dilute benzene solutions into methanol. After this procedure the polymer contains 0.03 wt % monomer *N*-vinylcarbazole, which interferes with the polymer fluorescence. A complete separation was achieved by means of quantitative gel permeation chromatography (system, Waters; column, μ-Styragel, 500 Å; dimension, 8 mm × 300 mm; solvent, benzene, spectrograde; detection, LC/UV, Pye Unicam). The polymer was not further fractionated in this study. Its weight-average molecular weight was $\bar{M}_w = 6 \times 10^4$.

***N*-(2-Hydroxyethyl)carbazolyl methacrylate** monomer was synthesized according to Percec et al.[51] It was copolymerized with butyl methacrylate in bulk in the presence of 2,2′-azobis(isobutyronitrile) at 50 °C. The mole fraction of carbazole units in the resulting copolymer was $x_{Cz} = 0.1$. Thus, those units may serve as a model for isolated fluorescence carbazole chromophores in a polymer environment (cf. Results, curve d in Figure 1).

The concentration of p-N-VCz in benzene solution used in this fluorescence study was generally 5×10^{-5} M (unit mol) (cf. Steady-State Measurements). The solutions were degassed in Pyrex vials by successive freeze–pump–thaw cycles on a high-vacuum line and transferred—with the aid of quartz to Pyrex sealed facilities—to quartz cells (Hellma QS 221, path length 10

mm) prior to spectroscopic measurements.

Instrumentation. Steady-State Measurements. Absorption spectra were measured on a Beckman Acta C III spectrophotometer. Stationary fluorescence spectra and fluorescence excitation spectra were recorded both on a Spex Fluorolog and on a Hitachi Perkin-Elmer MPF4 emission spectrometer. For the registration of fluorescence spectra a bandwidth of 2 nm was used. No correction with respect to emission wavelength dependent, nonlinear phototube responses (intensity vs. wavelength in arbitrary units) was applied. The sample temperature was controlled by a Haacke thermostat (25 °C). To minimize spectral distortions due to trivial reabsorption effects, the concentration was 5×10^{-5} M (unit mol), corresponding to an optical density of OD = 0.55 at the excitation wavelength λ_{exc} = 295 nm (cf. Results).

Transient Fluorescence Profiles and Analysis. Fluorescence profiles were recorded on a nanosecond time-correlated single-photon-counting apparatus of conventional configuration, which uses a thyratron-gated, hydrogen-filled flash lamp as the excitation source (PRA 3000, Photochemical Research Associates). Instrumental response functions of about 1.6 ns fwhm were routinely achieved by collecting the stray light of a Ludox scattering solution at the sample excitation wavelength. The samples were excited at λ_{em} = 295 nm by means of a Jobin-Yvon excitation monochromator, and the fluorescence was resolved by a Jobin-Yvon emission monochromator with slits set to give a 4–8-nm bandwidth. Alternatively, 10-nm band-pass interference filters (Balzers) were used to select the emission. Fluorescence photons were detected by a Hamamatsu Peltier cooled photomultiplier R928 and time correlated by conventional Ortec single-photon-counting electronics. Data were stored on a Tracor Northern TN1750 multichannel analyzer and then transmitted to a DEC PDP 11/23 computer and processed further.

A total of 15 000–20 000 counts was routinely collected in the peak channel. In order to detect a long-term time drift or changes in shape of the lamp profile associated with the long accumulation times (particularly for emission wavelengths longer than 440 nm and shorter than 370 nm, respectively), a repeated collection of lamp data was carried out at selected time intervals within the fluorescence data acquisition period. It turns out that the lamp with respect to its time drift and its shape profile can be considered to remain satisfactorily constant for the duration of the fluorescence accumulation. Nevertheless, a fully computer-controlled quasi-semisimultaneous collection of the lamp *and* the decay[52] would be undoubtedly more efficient to compensate for eventual time drifts and integral effects of data distortions. The fluorescence profiles were fitted to single-, double-, triple-, and four-exponential trial functions by the method of iterative reconvolution[53,54] using a χ^2 minimization procedure in a nonlinear regression algorithm of Marquardt.[55] The quality of fit was judged (a) by the reduced χ^2 criterion, (b) by visual inspection for randomized deviations in the weighted residuals as a function of channel number, (c) by the autocorrelation function of the weighted residuals, and (d) with respect to the stability of time constants T_i, while varying the start channel of fit in the rising edge of the experimental curve.[56] The energy-dependent time shift of photomultipliers must be considered to be a general problem in such measurements.[57] Undoubtedly the wavelengths at which the instrumental response function (λ_{exc} = 295 nm) and the excimer fluorescence (λ_{em} = 460 nm) are recorded differ considerably in our experiment. To partially overcome this possible convolution error in the leading edge and thus to resolve reliable data from the growth term of the E_2 fluorescence, both a fixed and an iterative shift procedure[58] was additionally introduced in least-squares fitting. However, the Hamamatsu R928 used in our system exhibits a relatively small wavelength dependence, as it has been pointed out by Ware et al.[59] in their recent study. Accordingly, corrections should be applied rather in the trailing edge to compensate for convolution errors.

III. Results

Photostationary Measurements. Curve a in Figure 1 shows the total fluorescence spectrum of p-N-VCz, 5×10^{-5} M (unit mol), in benzene solution which is typical for p-N-VCz prepared by cationic initiation. Following the arguments put forward by Itaya et al.,[34] the spectral

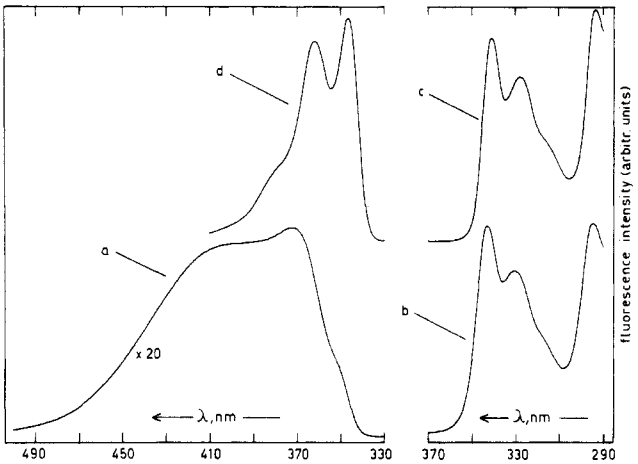

Figure 1. (a) Total fluorescence spectrum and (b) fluorescence excitation spectrum (λ_{em} = 420 nm) of cationically prepared p-N-VCz (5×10^{-5} M (unit mol) in degassed benzene (25 °C)). (d) Total fluorescence spectrum and (c) fluorescence excitation spectrum (λ_{em} = 380 nm) of *N*-(2-hydroxyethyl)carbazolyl–butyl methacrylate copolymer (x_{Cz} = 0.1 in benzene solution, 5×10^{-5} M in chromophore concentration (25 °C)). Spectra a and d are adjusted to fit on the same intensity scale. Sensitivity factor for (a): approximately 20×.

fluorescence pattern exhibits a relatively large contribution of the low-energy excimer E_2 (extrapolated band maximum approximately at 420 nm) which nearly equals the intensity of the high-energy, "partial overlap", excimer E_1 (peaking at 370 nm[29]) and which is due to the relatively high isotactic dyad mole fraction in this polymer. No wavelength dependence of the excimer fluorescence was found in the excitation spectrum (curve b) for $360 \leq \lambda_{em}/\text{nm} \leq 470$. Apart from the typical deviations regarding the intensity ratio of the $S_1 \leftarrow S_0$ and the $S_2 \leftarrow S_0$ transitions, respectively, the excitation spectrum of the polymer is essentially identical with its absorption spectrum, which is not shown here. The $^1L_b \leftarrow {}^1A$ band[60] shows a slight vibrational structure at 330 and at 343 nm which corresponds to the 0–0 transition. The band with its maximum near 295 nm represents the $^1L_a \leftarrow {}^1A$ transition.[60] The fluorescence excitation spectrum of p-N-VCz is within the limits of experimental error equal to the spectrum of a butyl methacrylate/*N*-(2-hydroxyethyl)carbazolyl methacrylate copolymer (curve c) containing only a small mole fraction of carbazole units (x_{Cz} = 0.1). Contrary to the excimer fluorescence behavior of the homopolymer p-N-VCz, the copolymer (5.0×10^{-5} M in chromophore concentration) exhibits vibrationally structured monomer fluorescence, exclusively, with the 0–0 transition of the $^1A \leftarrow {}^1L_b$ band—due to the small Stokes shift—near 348 nm (curve d in Figure 1). This is the result of an "intrachain dilution" of chromophores, which has been intensively studied in the case of p-1-VN and its copolymers with varying naphthalene mole fractions in the chain.[10–13] No comparative study has been reported so far with respect to p-N-VCz and its copolymers. Nevertheless, it can be concluded from Figure 1 that the "monomer-like" fluorescence of our copolymer reflects a situation where the excitation energy is localized at the carbazole chromophore within the macromolecular environment and where quite obviously an interchromophoric, intrachain interaction cannot proceed within the lifetime of the excited carbazole chromophore. On the other hand, the dominance of the excimer fluorescence of p-N-VCz leads to the conclusion that the electronic coupling between identical carbazole units and the dyad trap fraction presumably must be large. This observation is in accordance

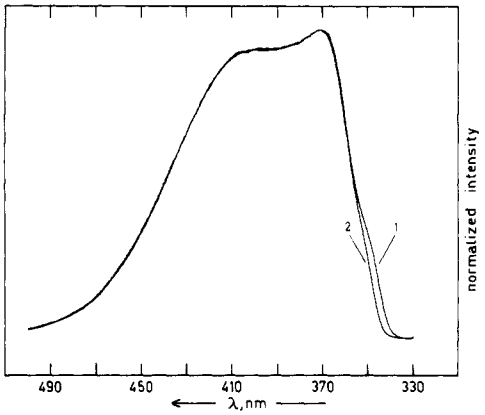

Figure 2. Total fluorescence of p-N-VCz in degassed benzene solution at 25 °C (excitation wavelength λ_{em} = 295 nm): (1) 5 × 10^{-5} M (unit mol); (2) 5 × 10^{-4} M (unit mol). The spectra are normalized to the maximum intensity at 370 nm. Sensitivity factor for (1): approximately 2×.

with the generally accepted view that the fluorescence of the primarily excited carbazole antenna—due to excitation transfer and irreversible trapping—contributes to a small extent only.[29,61] Particularly, in time-resolved fluorescence studies of p-N-VCz it has been pointed out[39,46] that no monomer emission is observable. This led to the discussion of a kinetic scheme that assumes a picosecond decay of the monomer fluorescence and thus permits one to disregard the monomer contribution on a nanosecond scale.

However, we want to emphasize that in sufficiently dilute systems p-N-VCz exhibits in fact a significant, nonnegligible monomer fluorescence at room temperature. The inspection of the fluorescence spectrum of p-N-VCz, 5 × 10^{-5} M (unit mol), reveals a distinct shoulder near 349 nm (curve a in Figure 1, which practically coincides with the 0–0 transition of the isolated carbazole moiety in the macrochain of the copolymer (curve d in Figure 1). Thus, we believe that this peak must be assigned to the 0–0 transition within the $^1A \leftarrow {}^1L_b$ monomer fluorescence band of p-N-VCz. Undoubtedly, the band is spectrally not pure and the peak shoulder indicates a slight superposition of interfering emissive high-energy species, which cannot be resolved from the spectral convolute of the steady-state emission.

On the other hand, in more concentrated p-N-VCz solution the intensity of this transition decreases and becomes in fact less significant. Figure 2 demonstrates this relation in an overlay representation. The spectra (curve 1, 5 × 10^{-5} M (unit mol); curve 2, 5 × 10^{-4} M (unit mol)) are normalized to the maximum intensity at 370 nm. We believe that the failure to observe emission from the excited monomer in 5 × 10^{-4} M (unit mol) p-N-VCz solution is due to the reabsorption of the relatively intense 0–0 transition within the ^1L_b band of the carbazole chromophore (curve b in Figure 1), which leads to a significant distortion in the short-wavelength region of its total fluorescence. This complication with respect to the fluorescence of carbazole double molecules had been already addressed by Johnson.[62]

Another important aspect results from a simple and approximative evaluation of fluorescence quantum yields. The comparison of intensities with respect to the 0–0 transitions of the monomer fluorescence (λ_{em} = 348 nm) between the homopolymer on the one side (curve a in Figure 1) and the copolymer on the other side (curve d in Figure 1) yields a normalized intensity of approximately 1/40. Since the fluorescence of the copolymer is not essentially quenched by the macromolecular environment of butyl methacrylate units, its intensity practically equals

Table I
Transient Fluorescence of p-N-VCz at λ_{em} = 348 nm: Best-Fit Decay Parameters[a]

amplitudes	sign	time constants, ns	% INT
M_2' = 0.45 (0.56)	+	T_2 = 0.49 (0.37)	7.01 (6.59)
M_3' = 0.13 (0.15)	+	T_3 = 2.41 (2.29)	9.90 (10.56)
M_4' = 0.06 (0.06)	+	T_4 = 32.92 (32.68)	66.63 (66.98)
M_5' = 0.05 (0.05)	+	T_5 = 9.47 (9.31)	16.46 (15.87)

[a] From the experimental data curve in Figure 3b; data maximum in channel 22; fit from channel 16 to channel 256. Values in parentheses are best fit parameters from simulated data based on the best fit parameters of the experimental curve in Figure 3b. χ^2_v = 1.06 (1.04).

that of an N-methylcarbazole solution of identical chromophore concentration (5.0 × 10^{-5} M in benzene). Assuming a fluorescence quantum yield of roughly $\varphi \cong 0.5$[63] for the quasi-isolated N-alkylcarbazole in the copolymer, the quantum yield for the monomer fluorescence of p-N-VCz can be estimated to be in the order of magnitude of $\varphi_F^M \cong 10^{-2}$. This relatively large value cannot be compatible with the generally accepted rapid picosecond monomer deactivation as the exclusive pathway, which means that in addition to this ultrafast trapping process, several slower events in the subnanosecond and nanosecond time regimes, respectively, must contribute to the decay of the monomer. It will be apparent from the following transient analysis that these relatively slow decay terms of the monomer fluorescence can be resolved.

Analysis of the Transient Profiles. The transient curves of cationically prepared p-N-VCz, 5 × 10^{-5} M (unit mol) in benzene, were recorded at λ_{em} = 348 nm, λ_{em} = 370 nm, and λ_{em} = 460 nm, respectively. Figure 3 shows the time-resolved fluorescence and its analysis in the monomer region of the peak shoulder near λ_{em} = 348 nm. Figure 3a shows the result of fitting with the sum of three exponentials. In this case a moderately good fit is obtained with a slight, but systematic deviation of the weighted residuals at the earliest time region (χ^2_v = 1.46). In Figure 3b the same experimental data convolution is fitted to a four-exponential form. This procedure leads to a significant improvement of the reduced χ^2 (χ^2_v = 1.06) and to a complete randomization of the weighted residuals and the autocorrelation function, respectively. In addition, the time constants remain essentially stable and no pronounced sensitivity has been observed while varying the starting channel of fit within the rising part of the experimental convolution pattern. The results of four-exponential data fitting at the emission wavelength λ_{em} = 348 nm are listed in Table I. The table contains the scaled relative amplitudes, M', the signs of the respective M' values, the best fit time constants evaluated by the χ^2 criterion, and the relative intensity, % INT, of the components contributing to the fluorescence profile. The best fit time constants are found to be $T_2 \cong 0.5$ ns, $T_3 \cong 2.4$ ns, $T_4 \cong 32.9$ ns, and $T_5 \cong 9.5$ ns, respectively. Hereafter in our nomenclature the term T_1, which is indeed not resolvable from our measurements but which is taken into account in the kinetic treatment (cf. next section), will be reserved for the picosecond time domain. The values in parentheses show the best fit of the synthetic convolution between the instrumental response (lamp function in Figure 4) and the artificial curve generated with the best fit decay parameters of the experimental data. Accuracies of best fit time constants and amplitudes are found to be within the limit of such a procedure. This result may indicate the reliable accuracy of the fit routine—despite the rather serious problems of freely adjustable parameters in a four-exponential fit.

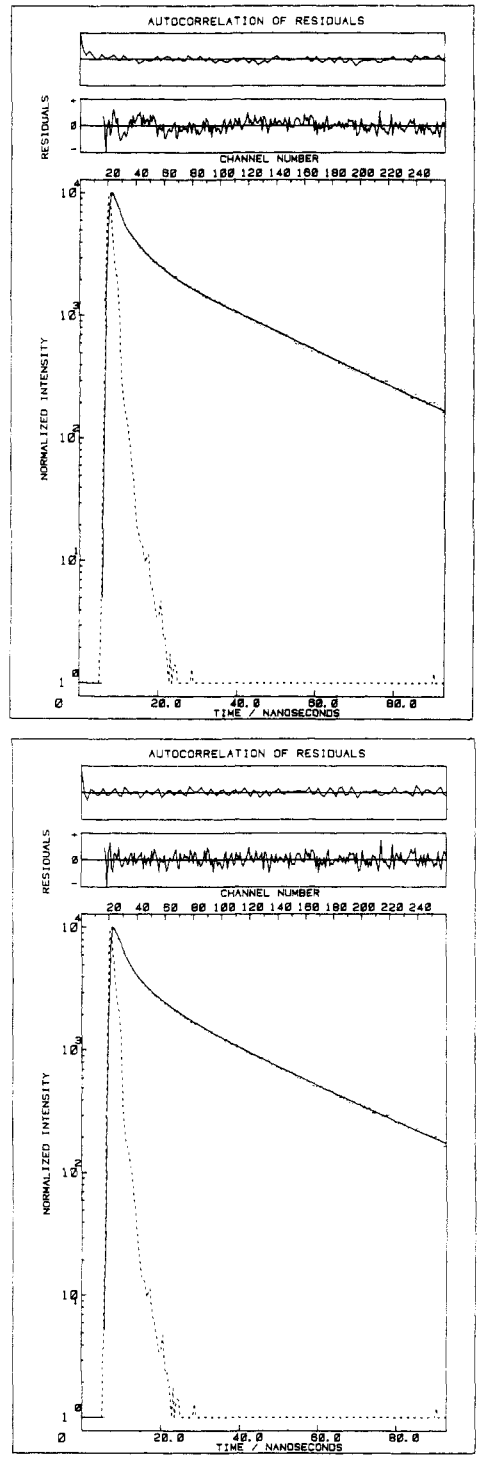

Figure 3. Fluorescence profile of p-N-VCz (5×10^{-5} M (unit mol) in degassed benzene (25 °C)) (emission wavelength λ_{em} = 348 nm): (---) experimental response function; (···) experimental data. (a) Solid line shows best fit to a three-exponential function according to $F_{348}(t) = 0.47 \exp(-t/0.70\text{ ns}) + 0.10 \exp(-t/5.56\text{ ns}) + 0.07 \exp(-t/31.19\text{ ns})$; $\chi^2_v = 1.46$; time scale 0.4 ns/channel; fit from channel 16 to channel 256. (b) Solid line shows best fit to a four-exponential function according to eq I, with decay parameters listed in Table I.

Therefore, from the results of our data fit, we must suggest that the fluorescence profile at λ_{em} = 348 nm, $F_{348}(t)$, which to a major part contains the monomer decay, can be satisfactorily described by a sum of four exponentials according to

$$F_{348}(t) \approx M_2' \exp(-t/T_2) + M_3' \exp(-t/T_3) + M_4' \exp(-t/T_4) + M_5' \exp(-t/T_5) \quad \text{(I)}$$

Table II
Time-Resolved Low-Energy Excimer Fluorescence at λ_{em} = 460 nm: Best-Fit Growth and Decay Parameters[a]

amplitudes	sign	time constants, ns	% INT
C_2' = 0.12 (0.14)	-	T_2 = 0.35 (0.28)	1.10 (1.04)
C_3' = 0.01 (0.01)	-	T_3 = 3.18 (2.51)	0.77 (0.79)
C_4' = 0.10 (0.10)	+	T_4 = 35.38 (35.36)	98.13 (98.17)

[a] From the experimental data curve in Figure 4c; data maximum in channel 49; fit from channel 20 to channel 256. Values in parentheses are best fit parameters from simulated data based on the best fit parameters of the experimental curve in Figure 4c. χ^2_v = 1.07 (1.04).

where the coefficients M' of each term have a positive sign (cf. Table I).

Next we will examine the ultimate range in the long-wavelength excimer fluorescence of p-N-VCz, which seems to arise solely from the low-energy, "sandwich" singlet excimer E_2. Typical data and computer fits to the experimental pattern at the emission wavelength λ_{em} = 460 nm are presented in Figure 4. Figure 4a shows the fitted fluorescence profile of E_2 with a time resolution of 0.4 ns/channel. The decay is adequately described by a single-exponential function, corresponding to a time constant which is, within the experimental error of ±5%, identical with T_4, resolved from the monomer fluorescence decay at 348 nm (cf. Table I), namely, $T_4 \cong 34.5$ ns. The very same value for T_4, as well as a strictly monoexponential behavior, is found in independent experiments by following the decay over a time period of more than 2 decades (time resolution, 0.8 ns/channel).

As to the leading edge of the fluorescence convolution pattern in Figure 4a, the results of fit procedures reveal strong evidence for a significant biphasic growth term (see the approximate buildup parameters, quoted in caption of Figure 4a). Since it has turned out that even on a relatively short total time scale of about 50 ns the long time constant T_4 could be evaluated accurately, without any sensitivity toward the variation of the starting channel in the course of fit procedures, the time resolution was chosen to be 0.2 ns/channel for a more refined analysis. In Figure 4b,c the fluorescence profiles of E_2 are displayed on a time basis of 0.2 ns/channel. Figure 4b shows the experimental data optimally fitted to a two exponential, consisting of one growth term (negative amplitude) with an approximative rise time of $T_{rise} \cong 2.07$ ns and of one decay term (positive amplitude) associated with the long time constant T_4, according to $T_4 \cong 35.5$ ns. This experimental data fit agrees satisfactorily with the 2.6-ns rise time in E_2 fluorescence reported by Phillips et al.[39] and the approximate 2.0-ns buildup time published by Tagawa et al.[64] However, although the randomness of the residuals can be accepted on the 95% confidence level (χ^2_v = 1.35), it becomes already apparent by visual inspection that the weighted residuals and the autocorrelation function exhibit a pronounced oscillation in the early time channels of the rise curve. In Figure 4c the same data of convoluted E_2 fluorescence are fitted to a triple-exponential response which contains two buildup terms and one decay term, respectively. In any respect, the double-exponential fit of the rising part will lead to a significant improvement, as shown by the goodness of fit criteria (χ^2_v = 1.07), stochastic distribution of the weighted residuals, and complete randomization of their autocorrelation. A listing of best fit parameters, analogous to that in Table I, is given in Table II for the fluorescence pattern of E_2 at λ_{em} = 460 nm. However, the evaluation of these data has been difficult due to the strongly differing intensity contributions of the components in different domains of the time scale. Best

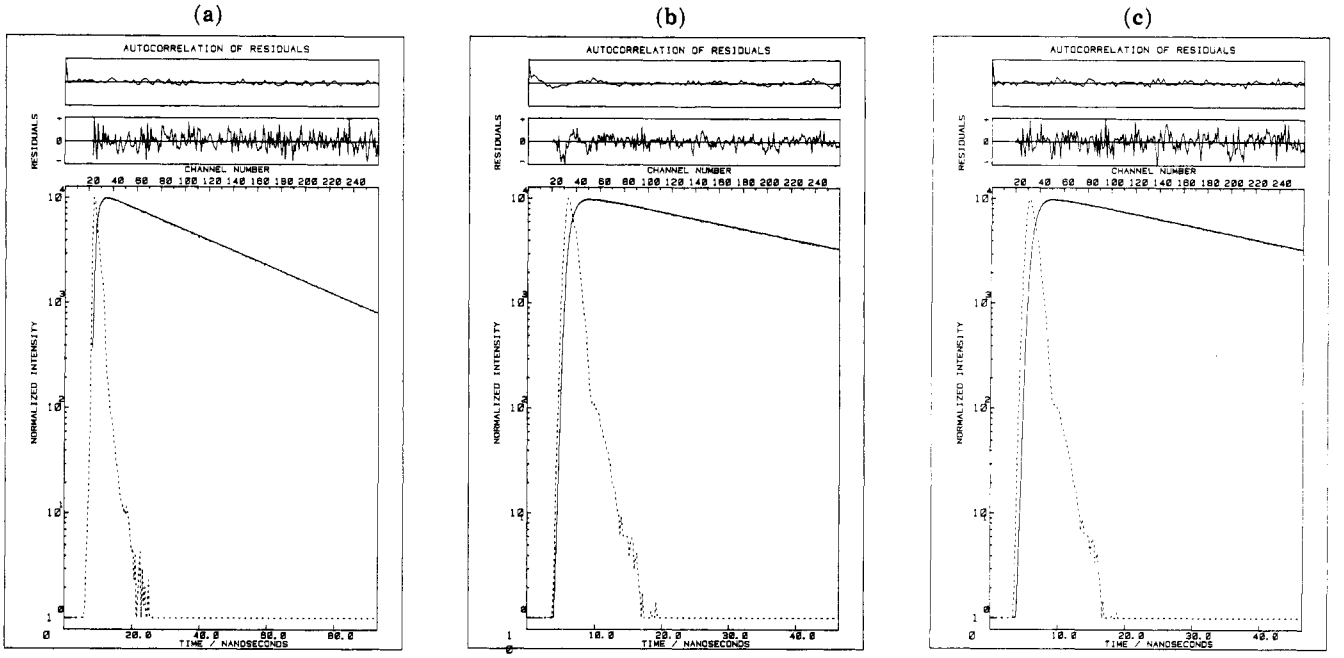

Figure 4. (a) Fluorescence profile of p-N-VCz (5×10^{-5} M (unit mol) in degassed benzene (25 °C)) (emission wavelength λ_{em} = 460 nm; time scale 0.4 ns/channel): (---) lamp; (···) experimental curve; (—) three-exponential fit according to $F_{460}(t) = -0.43 \exp(-t/0.12$ ns) $- 0.02 \exp(-t/1.13$ ns) $+ 0.19 \exp(-t/34.6$ ns); $\chi^2_v = 1.18$; fit from channel 23 to channel 256. Transient fluorescence curve of p-N-VCz (5×10^5 M (unit mol) in degassed benzene (25 °C)) (λ_{em} = 460 nm; time scale 0.2 ns/channel): (---) lamp function; (···) convoluted experimental data. (b) Solid line shows computed best fit to a biexponential form according to $f_{460}(t) = -0.02 \exp(-t/2.07$ ns) + 0.10 $\exp(t/35.5$ ns); $\chi^2_v = 1.35$; fit from channel 20 to channel 256. (c) Solid line shows best fit triple-exponential curve according to eq II, with rise and decay parameters listed in Table II.

fit time constants are evaluated to $T_2 \cong 0.4$ ns, $T_3 \cong 3.0$ ns, and $T_4 \cong 35$ ns, respectively, with two negative, preexponential coefficients C_2' and C_3' and one positive amplitude C_4'. Within the experimental error their values are identical with the time constants T_2, T_3, and T_4 of the monomer decay (Table I), which justifies the choice of the indices 2, 3, and 4 and simultaneously indicates their apparent correlation. The ratios of the scaled relative amplitudes are found to be approximately $C_2'/C_3' \approx 10$ and $C_2'/C_4' \approx 1$, respectively, which is of course to some degree dependent on the time shift of the lamp function (cf. Experimental Section, channel shift optimization). The values in parentheses represent the best fit parameters of the simulated convolution, which consists of the experimental lamp function and the respective synthetic triple-exponential function generated on the basis of the best fit parameters of the experimental curve (Table II).

We believe, therefore, that the theoretical molecular response of E_2 at λ_{em} = 460 nm can be best approximated by a double-exponential rise curve and a monoexponential decay term, respectively, according to

$$F_{460}(t) \cong F_{E_2}(t) \approx -C_2' \exp(-t/T_2) - C_6' \exp(-t/T_3) + C_4' \exp(-t/T_4) \quad \text{(II)}$$

The results of multiexponential fitting to the transient data at the emission wavelength λ_{em} = 370 nm are given in Figure 5. This region corresponds to the maximum fluorescence intensity, which is due to the contribution of E_1[29] and presumably to the additional superposition of other high-energy trap species. Figure 5a shows the triple-exponential fit of the data with three apparent decay times of 1.3, 7.3, and 32.6 ns, respectively. Nevertheless the reduced χ^2 is relatively large, $\chi^2_v = 1.22$, and both the weighted residuals and the autocorrelation show a significant systematic deviation. A four-exponential fit (Figure 5b) yields an essential improvement, namely, $\chi^2_v = 1.00$ and a satisfactory randomization of the residuals and their autocorrelation function. The best fit decay

Table III
Transient High-Energy Trap Fluorescence at λ_{em} = 370 nm: Best-Fit Decay Parameters[a]

amplitudes	sign	time constants, ns	% INT
$D_2' = 0.57$ (0.66)	+	$T_2 = 0.66$ (0.38)	5.35 (3.67)
$D_3' = 0.28$ (0.37)	+	$T_3 = 2.60$ (2.05)	10.42 (11.12)
$D_4' = 0.14$ (0.14)	+	$T_4 = 33.88$ (34.12)	68.34 (67.95)
$D_5' = 0.10$ (0.12)	+	$T_5 = 10.64$ (10.13)	15.89 (17.26)

[a] From the experimental data curve in Figure 5b; data maximum in channel 24; fit from channel 24 to channel 256. Values in parentheses are best fit parameters from the simulated convolutions based on the best fit parameters of the experimental curve in Figure 5b. $\chi^2_v = 1.00$ (0.98).

parameters are given in Table III. Again, the best fit parameters of the simulated curve are given in parentheses. The time constants T_2, T_3, T_4, and T_5 are approximately recovered from this analysis. However, it must be noted that the data fit at λ_{em} = 370 nm is, in general, more difficult. Thus, the incorporation of the rising edge yields to a dramatic increase of χ^2_v, though this procedure causes only a moderate variation with respect to the relaxation times.

Apart from these four exponential decays terms, no rise term could be resolved. As a consequence the high-energy trap fluorescence at λ_{em} = 370 nm may be represented by the empirical relationship

$$F_{370}(t) \approx D_2' \exp(-t/T_2) + D_3' \exp(-t/T_3) + D_4' \exp(-t/T_4) + D_5' \exp(-t/T_5) \quad \text{(III)}$$

with D_2', D_3', and D_5' all positive.

IV. Kinetic Model

In order to develop a kinetic scheme, we will first summarize and discuss the experimental results. The first important observation concerns the fact that no nanosecond delay could be resolved from the rising edge of the fluorescence profile at the wavelength λ_{em} = 370 nm (cf. Figure 5, Table III, and eq III). The absence of a growth

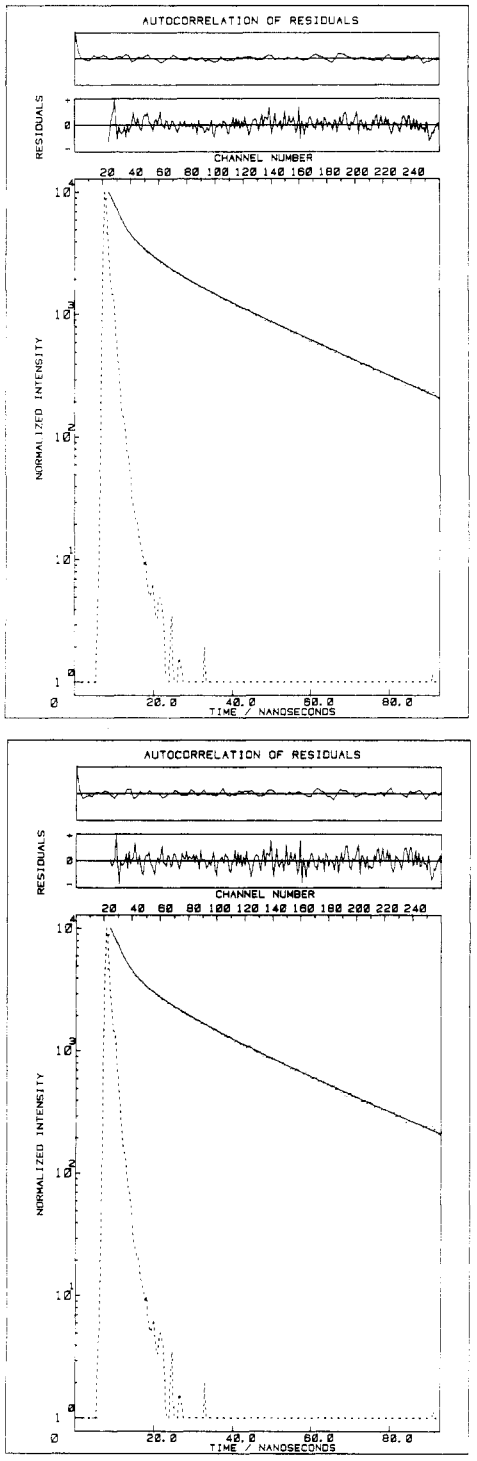

Figure 5. High-energy trap fluorescence of p-N-VCz (5×10^{-5} M (unit mol) in degassed benzene (25 °C)) (λ_{em} = 370 nm; time scale 0.4 ns/channel): (- - -) instrumental response; (···) experimental curve. (a) Solid line shows best fit to a triple-exponential form corresponding to $F_{370}(t) = 0.58 \exp(-t/1.32\ \text{ns}) + 0.16 \exp(-t/7.30\ \text{ns}) + 0.15 \exp(-t/32.60\ \text{ns})$; $\chi^2_v = 1.22$; fit from channel 24 to channel 256. (b) Solid line shows best fit four-exponential curve according to eq III, with decay parameters quoted in Table III.

term is indicative of a rapid picosecond population of quasi preformed high-energy traps. Thus, in the early stage of trapping the isolated chromophores of the monomeric type are quite rare and deactivate on a picosecond time scale. However, while the high-energy emission (λ_{em} = 370 nm) has its origin in preformed traps with rise terms not resolvable by nanosecond detection and deconvolution routines, a striking result from the transient curve of the

Scheme I

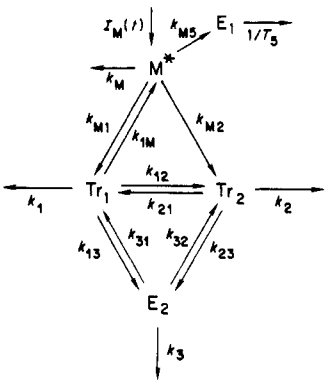

low-energy excimer E_2 concerns the observation of a pronounced delay following the excitation pulse (cf. Figure 4c, Table II, and eq II): This means that E_2 needs time to be populated, whereby the time constants T_2 and T_3 may be interpreted to refer to conformational changes to meet the structural requirement for the totally eclipsed conformation of E_2. Within this picture, the biexponential population pattern of E_2 reflects a series of multiple relaxation steps from preformed high-energy traps (not be confused with E_1) to low-energy traps induced by side-chain motions, in which the carbazole chromophore pair intermediates, as a result of increasing overlap, gain increasing stability. As a rough approximation of these rather complex events, we may treat the mechanism of E_2 population in terms of a formal, macroscopic interaction between distinct traps, on the one hand, and the sandwich dimer E_2, on the other hand. Starting from the principle according to which the number of experimentally observed exponentials must equal the number of interacting states in a time-independent rate constant formalism, we have to interpret our numerically resolved triple-exponential function in eq II (see also Figure 4c and Table II) as the consequence of three interconvertible kinetic entities. A kinetic scheme which seems appropriate for the description of the p-N-VCz system is proposed in Scheme I, where M* represents the excited monomeric carbazole chromophore and E_1 and E_2 symbolize the spectrally distinct and structurally assigned excimers of the high-energy "partial overlap" type and the low-energy "sandwich" type, respectively.

According to the results of recent investigations on dimeric models for E_1 and E_2,[32] we may disregard any interaction in which E_1 is formed from or converted to E_2. Due to these results, and with respect to our situation of having to explain a triple-exponential profile in eq II, we have to introduce *two* novel traps, Tr_1 and Tr_2, respectively. Thus, Tr_1 and Tr_2 are considered to be two kinetically distinct high-energy traps. Presumably, they occur in isotactic configurations and at least one of them will spectrally overlap with E_1 in the region of its maximum fluorescence intensity (λ_{em} = 370 nm). Detrapping is an inportant concept in this scheme; thus, Tr_1 is assumed to be a shallow trap, which shows dissociative behavior, while Tr_2 is treated as a deep trap. The scheme represents an extended version of the mechanism proposed by Phillips et al.[39] in which one of the traps can be identified with the third excimer postulated by these authors. Since the high-energy fluorescence profiles exhibit no significant time delay in the subnanosecond and in the nanosecond domain (cf. Figure 5b, Table III, and eq III), we assume that both traps Tr_1 and Tr_2, just as E_1, should be directly populated from the excitonic monomeric state on a picosecond time scale. The trapping rate constants k_{M5}, k_{M1}, and k_{M2}, in

a first approach (cf. Discussion), are assumed to be exponentialized, each containing the diffusive energy transport and the concentration of the respective preformed site along the polymer chain. On the other hand, the significant nanosecond delay in the leading edge of Figure 4c indicates that the direct picosecond evolution of the low-energy excimer E_2 from the excited monomer, M*, via excitation transfer and trapping in E_2-forming sites, quasi prior to excitation, seems to be a rather rare event and thus can be neglected. As to the population of E_2, we take into account two independent, energy cascading pathways in the nanosecond time domain, with rate constants k_{13} and k_{23}, respectively. The rate constants k_{31} and k_{32} allow for the reversibility of these steps; they correspond to the processes regenerating the excited traps Tr_1 and Tr_2, respectively. For the most general situation in the kinetic treatment of the downhill process, we assume the traps Tr_1 and Tr_2 to be interrelated to each other, with rate constants k_{12} and k_{21}, respectively. The rate constant k_M reflects the decay rate of the isolated carbazole chromophore, M*, by radiative and nonradiative processes in the absence of energy transport. The rate constants k_1, k_2, and k_3 are the reciprocal hypothetical effective lifetimes of the fluorescent traps Tr_1, Tr_2, and E_2, respectively, in the absence of gain terms and further loss terms. Finally, the rate constant $1/T_5$ is used to represent the rate at which E_1 deactivates via radiative and nonradiative channels.

As to the picosecond genesis of the electronically excited traps E_1, Tr_1, and Tr_2, it is evident that their evolution must correspond to the overall picosecond decay of the excited monomer M*. Nevertheless, it is an experimental fact that the steady-state spectrum shows a significant and relatively intense monomer fluorescence (Figure 1, curve a, Figure 2, curve 1; peak shoulder at λ_{em} = 349 nm). Moreover, the transient analysis of the fluorescence at λ_{em} = 348 nm, which to a major part contributes to the monomeric type, reveals a pronounced multiexponential nanosecond relaxation profile with a characteristic long-time behavior (Figure 3b, Table I, and eq I), in addition to the nonresolvable picosecond decay. In any case, both experimental results strongly indicate that the excited monomeric state, M*, apart from its irreversible picosecond deactivation into preformed traps, must be coupled to a gain term. Hence, we take into account the dissociation of Tr_1 as a nonnegligible and important source term for the delayed repopulation of the carbazole chromophore, M*. The rate constant k_{1M} corresponds to the rate of dissociation of Tr_1 to yield excited, "monomeric" traps.

For the calculation of their decay laws we replace M*, Tr_1, Tr_2, and E_2 in the scheme by the time variables $m(t)$, $x(t)$, $y(t)$, and $z(t)$, respectively. Taking

$$k_M + k_{M1} + k_{M2} + k_{M5} = a_{MM}$$
$$k_1 + k_{12} + k_{13} + k_{1M} = a_{11} \qquad (1.1)$$
$$k_2 + k_{21} + k_{23} = a_{22} \qquad k_3 + k_{31} + k_{32} = a_{33}$$

and

$$k_{1M} = a_{M1}, \quad k_{M1} = a_{1M}, \quad k_{21} = a_{12},$$
$$k_{31} = a_{13}, \quad k_{M2} = a_{2M}, \quad k_{12} = a_{21}, \qquad (1.2)$$
$$k_{32} = a_{23}, \quad k_{13} = a_{31}, \quad k_{23} = a_{32}$$

and neglecting the source term of the exciting light, $I_M(t)$, within the approximation of a δ-pulse excitation, the evolution equations can be written

$$\dot{m}(t) + a_{MM}m(t) - a_{M1}x(t) = 0 \qquad (2.1)$$
$$\dot{x}(t) + a_{11}x(t) - a_{12}y(t) - a_{13}z(t) - a_{1M}m(t) = 0 \qquad (2.2)$$
$$\dot{y}(t) + a_{22}y(t) - a_{21}x(t) - a_{23}z(t) - a_{2M}m(t) = 0 \qquad (2.3)$$
$$\dot{z}(t) + a_{33}z(t) - a_{31}x(t) - a_{32}y(t) = 0 \qquad (2.4)$$

Assuming linear kinetics the solutions of eq 2.1–2.4 take the general form

$$m(t) = \sum_k M_k \exp(-t/T_k) \qquad (3.1)$$
$$x(t) = \sum_k A_k \exp(-t/T_k) \qquad (3.2)$$
$$y(t) = \sum_k B_k \exp(-t/T_k) \qquad (3.3)$$
$$z(t) = \sum_k C_k \exp(-t/T_k) \qquad (3.4)$$

with k = 1–4; the reciprocal time constants, $1/T_k$, principally follow as real solutions

$$1/T_1 > 1/T_2 > 1/T_3 > 1/T_4 \qquad (4)$$

from the eigenvalue problem of the secular determinant

$$\begin{vmatrix} -(1/T + a_{MM}) & -a_{M1} & 0 & 0 \\ -a_{1M} & -(1/T + a_{11}) & -a_{12} & -a_{13} \\ -a_{2M} & -a_{21} & -(1/T + a_{22}) & -a_{23} \\ 0 & -a_{31} & -a_{32} & -(1/T + a_{33}) \end{vmatrix} = 0 \qquad (5)$$

Using some algebra and taking into account the initial conditions $m(t = 0) = m(0)$, $x(t = 0) = 0$, $y(t = 0) = 0$, and $z(t = 0) = 0$, where $m(0)$ is the maximum population number of the excited monomeric donor, one finds that subsequent to the δ pulse, the normalized amplitudes and their linear functional relations are

$$M_k/m(0) = h_k A_k/m(0) \qquad (6.1)$$
$$C_k/m(0) = i_k A_k/m(0) \qquad (6.2)$$
$$B_k/m(0) = j_k A_k/m(0) \qquad (6.3)$$

with k = 1–4 and where the linear coefficients h_k, i_k, and j_k contain the rate constants, given in (1.1) and (1.2) and the reciprocal time constants, $1/T_k$, which follow from the secular equation, (5), whereas

$$A_k/m(0) = G(\bar{h}_k, \bar{i}_k, \bar{j}_k) \qquad (7)$$

contains difference quantities $\bar{h}_k$, $\bar{i}_k$, and $\bar{j}_k$ between different h_k's, i_k's, and j_k's, respectively. A detailed analysis and the analytical expressions for the linear coefficients are available as supplementary material.

From eq 6 and 7, together with the formulas derived in the supplementary material each of the relative amplitudes is now calculable, and thus the theoretical time profiles $m(t)$, $x(t)$, $y(t)$, and $z(t)$ can be interpreted.

Finally, the population profile of the high-energy excimer E_1 can be calculated. Setting $k_{M5} = a_{5M}$ and using $m(t)$ (supplement) as well as the boundary condition $E_1(t = 0) = 0$, the expression takes the form

$$E_1(t) = -a_{5M}\sum_{k=1}^{4}(1/T_k - 1/T_5)^{-1}M_k \exp(-t/T_k) + a_{5M}\exp(-t/T_5)\sum_{k=1}^{4}(1/T_k - 1/T_5)^{-1}M_k = \sum_{k=1}^{4}D_k \exp(-t/T_k) + D_5 \exp(-t/T_5) \qquad (8)$$

which is a five-exponential result.

V. Discussion

The kinetic scheme shown in Scheme I may be hypothesized from the analysis of the transient fluorescence curves (a) in the monomer region (cf. Figure 3b, Table I, and eq I), (b) in the high-energy excimer region, which corresponds to the intensity maximum of the total

fluorescence (cf. Figure 5b, Table III, and eq III), and (c) in the spectral range of the low-energy excimer E_2 (cf. Figure 4c, Table II, and eq II). The model accounts for both well-defined excimer states E_1 and E_2 and, in addition, takes into consideration *two* kinetically distinct but structurally undefined "excimer-like" traps Tr_1 and Tr_2, respectively. These are representative for the presumably large number of excimer-forming sites, which are not further resolvable due to the finite time resolution of our transient apparatus and because of the limitations of sensitivity with respect to the multidimensional minimization in our fit routines. In analogy to E_1,[29] both traps Tr_1 and Tr_2 can be assumed to be a preformed chromophore pair of slightly different geometry and energy with relatively large equilibrium fractions in the isotactic configurational domain. Owing to the efficient excited-state transport their electronic excitation is expected to occur on a picosecond time scale. Time is implicitly confirmed from the results of our transient curve analysis in the high-energy region at λ_{em} = 370 nm (Figure 5b, Table III, and eq III), inasmuch as at least no resolvable time delay could be deconvoluted. However, due to the partial cancellation of growth and decay terms, respectively, the analysis of both the picosecond source term of the high-energy traps (E_1, Tr_1, and Tr_2) and the picosecond decay term of the monomeric carbazole unit, M*, is difficult in general and has not been carried out so far.

Apart from these picosecond events to trap excitation and monomer deactivation, there is another important aspect. The steady-state spectra of sufficiently dilute p-N-VCz solutions exhibit a significant peak shoulder near 348 nm (cf. Figure 1, curve (a, and Figure 2, curve 1), which is to be attributed to an intrachain monomeric state. Therefore, we want to note that the monomer fluorescence of p-N-VCz represents an intrinsic property of this polymer, which cannot be neglected in the kinetic treatment of its excited-state dynamics. In order to harmonize the picosecond events of electronic energy transfer between excited monomer, M*, and the high-energy traps, on the one hand, with the relatively intense 0–0 transition of the monomer fluorescence from the stationary experiment, on the other hand, we must take into account the concept of reversibility between one and the other high-energy trap and the excited monomeric state, respectively. While Tr_2 is treated as a "deep" trap, we must propose that Tr_1 exhibits dissociative behavior to yield the "monomeric trap" in the reverse step. The rate of dissociation, $a_{M1}x(t)$, has therefore a considerable influence for the repopulation of M* (cf. eq 2.1). Since Tr_1 itself is involved in a complex subnanosecond and nanosecond interaction between Tr_2 and E_2 (vide infra), this complicated dynamics is reflected in the source term, $a_{M1}x(t)$, and causes a multiexponential "long-time" behavior in the monomer fluorescence decay, in addition to its picosecond deactivation. The time-resolved analysis in the monomer region (cf. Figure 3b, Table I, and eq I) reveals one subnanosecond component T_2 and two nanosecond time constants T_3 and T_4 whereas the picosecond decay and its time constant T_1 cannot be resolved. The remaining nanosecond component corresponding to $T_5 \cong 10$ ns is presumably the result of a spectral overlap of M* and E_1 and we believe that T_5 represents the effective lifetime of this relatively isolated electronic trap species. Nevertheless, its intensity–time profile is essentially more complex, as it follows from eq 8. This will be discussed below from the transient data at the emission wavelength λ_{em} = 370 nm.

The formal kinetic interrelation of the traps Tr_1 and Tr_2 and E_2, as a consequence of electronic energy dissipation biased by the segmental dynamics of the chain, gains particular significance from the transient curve of E_2 (Figure 4c), which is free from interfering emissive high-energy trap contributions. While the picosecond term T_1 corresponding to the population of the high-energy traps is not resolvable, we obtain quasi-identical time constants T_2 and T_3 with negative amplitudes C_2' and C_3', respectively, and T_4 connected to an amplitude C_4' with a positive sign (cf. Table II and eq II).

The transient analysis at λ_{em} = 370 nm (cf. Figure 5b, Table III, and eq III) is rather complicated because of the presumable spectral superposition of photons. These are emitted from the hypothetical traps Tr_1 and Tr_2, which interfere with the emission profile of the high-energy excimer E_1 and cannot be discriminated by single-photon-counting detection. On the other hand, the contribution of the excited monomer is rather small and can be disregarded. Nevertheless we recover T_2, T_3, and T_4 and again observe T_5, which is considered to be the decay time of E_1—very similar to that reported by Phillips et al.[46] Again no picosecond term due to the growth of the high-energy trap population can be resolved, and all amplitudes of this four-exponential fit are found to be positive.

In order to examine the validity of the proposed kinetic scheme we have to compute the time constants T_k, as well as the normalized amplitudes $M_k/m(0)$, $A_k/m(0)$, $B_k/m(0)$, $C_k/m(0)$, and $D_k/m(0)$, respectively, from eq 15–18 and 20 in the supplement. These have to be compared with those which follow from the numerical fits of the experimental fluorescence patterns in eq I–III. According to the character of the secular determinant it is clear that there cannot exist four real solutions $1/T_1$, $1/T_2$, $1/T_3$, and $1/T_4$, respectively, for each combination of freely varying rate constants. With the conditions

$$1/T_1 > 1/T_2 > 1/T_3 > 1/T_4$$

and the inequality

$$1/T_1 > a_{MM} > a_{11} > 1/T_2 > a_{22} > 1/T_3 > a_{33} > 1/T_4$$

we obtain in general a variety of computed profiles, which are—at least with respect to the sign of the amplitudes—in satisfactory accordance with the experimental data. A typical set of trial data, including the fixed reciprocal effective lifetimes k_M, k_1, k_2, and k_3, respectively,[65] is given in Table IV. From eq 15, 8.2, 9.2, 10.2, and 16 (supplement) we find $A_1/m(0)$ negative and $A_2/m(0)$, $A_3/m(0)$, and $A_4/m(0)$ positive, and with eq 20.1–20.4, $M_1/m(0)$, $M_2/m(0)$, $M_3/m(0)$, and $M_4/m(0)$ all positive. Thus, the theoretical response function of the monomer decay $I_M(t)$, $m(t)$, shows a pure decay behavior with four positive amplitudes, which is essentially identical with the experimental result (cf. eq I, Table I, and Figure 3b), with the limitation, however, that the picosecond term containing the parameters $M_1/m(0)$ and T_1 is experimentally not resolvable whereas the term M_5', associated with the exponential of time constant $T_5 \cong 10$ ns, presumably belongs to the decay of E_1 as a result of spectral overlap. In addition, the contributions of the computed relative amplitudes $M_3/m(0)$ and $M_4/m(0)$ are too small. Due to the extremely sensitive interrelation between $1/T_4$, k_{13}, k_{31}, k_{23}, and k_{32}, respectively, application of iterative computer procedures, in principle, might lead to better agreement.

The transient population profile $E_1(t)/m(0)$ of the high-energy excimer E_1 is calculated from eq 20. With $M_1/m(0)$, $M_2/m(0)$, $M_3/m(0)$, $M_4/m(0)$ all positive and with the condition

$$1/T_1 > 1/T_2 > 1/T_3 > 1/T_5 > 1/T_4$$

where $T_5 \cong 10$ ns is the experimentally observed value (see

Table IV
Transient Population and Deactivation Profiles of M*, Tr_1, Tr_2, E_2, and E_1: Kinetic Test Data

k_M	0.83000E+08[a,d]	k_{12}	0.20000E+08
k_{M1}	0.80000E+11	k_{21}	0.40000E+09
k_{1M}	0.90000E+10	k_3	0.22000E+08[b,d]
k_{M2}	0.60000E+10	k_{13}	0.36000E+10
k_{M5}	0.10000E+11	k_{31}	0.28000E+08
k_1	0.83000E+08[a,d]	k_{23}	0.40000E+08
k_2	0.83000E+08[a,d]	$1/T_5$	0.10000E+09[c,d]
$1/T_1$	0.10397E+12	$1/T_3$	0.47897E+09
a_{MM}	0.96083E+11	a_{22}	0.52300E+09
$1/T_2$	0.48848E+10	$1/T_4$	0.29462E+08
a_{11}	0.12703E+11	a_{33}	0.54000E+08

term	T_k, ns	$M_k/m(0)$	$A_k/m(0)$	$B_k/m(0)$	$C_k/m(0)$	$D_k/m(0)$
1	0.00962	0.9204764	−0.8066194	−0.0532335	0.0256155	−0.0886183
2	0.20472	0.0779418	0.7897943	−0.1102975	−0.5876518	−0.1628944
3	2.08781	0.0011585	0.0123061	0.1526839	−0.1186182	−0.0305690
4	33.94152	0.0004234	0.0045188	0.0108470	0.6806550	0.0600252
5	10.00000[c,d]					0.2220566

[a-c] See ref 65. [d] Fixed rate constants.

Table III), we obtain $D_1/m(0)$, $D_2/m(0)$, and $D_3/m(0)$ all negative whereas $D_4/m(0)$ and $D_5/m(0)$ are obtained as positive quantities (cf. last column in Table IV). Apart from the nonresolvable picosecond growth term (rise time T_1), the empirical equation (III) (see also Table III and Figure 5b) quite obviously does not fit the theoretical pattern. While T_4 and T_5 are correctly attributed to decay terms (positive sign of amplitudes D_4 and D_5, respectively), it becomes apparent that the time constants T_2 and T_3—theoretically expected as rise times from eq 8—are experimentally found to be decay time constants connected to positive amplitudes D_2' and D_3', respectively. This is due to the spectral superpositon of E_1 with the dimer traps Tr_1 and Tr_2, which leads to the simultaneous observations of several distinct photon species. Since we calculate a negative value for $B_2/m(0)$ and a positive value for $B_3/m(0)$ from (17) and (10.2) (supplement), in addition to the positive quantities of $A_2/m(0)$ and $A_3/m(0)$, it turns out that the sum of their positive amplitudes $(A_2 + B_2)/m(0)$ and $(A_3 + B_3)/m(0)$ exceeds the negative values $D_2/m(0)$ and $D_3/m(0)$. Nevertheless, a more detailed analysis of a situation corresponding to three emitting species, spectrally superimposed in a coupled system, in general seems to be intractable, and no conclusions regarding the ratios of experimental amplitudes should be drawn at $\lambda_{em} = 370$ nm. On the other hand, the experimentally observed transient fluorescence pattern of the low-energy excimer E_2 is spectrally pure. With $A_1/m(0)$ negative and $A_2/m(0)$, $A_3/m(0)$, and $A_4/m(0)$ all positive, from (18) and (9.2) (supplement) we calculate $C_1/m(0)$ positive, $C_2/m(0)$ negative, $C_3/m(0)$ negative, and $C_4/m(0)$ positive. Thus, $I_{E_2}(t)$, the molecular response function of E_2, which is proportional to the profile $z(t)$ in eq 5.4 (supplement) yields

$$I_{E_2}(t) \propto C_1/m(0)\exp(-t/T_1) - C_2/m(0)\exp(-t/T_2) - C_3/m(0)\exp(-t/T_3) + C_4/m(0)\exp(-t/T_4)$$

a nonresolvable picosecond decay term, *two* growth terms, corresponding to the rise times T_2 and T_3, respectively, and one decay term, which contains the asymptotic behavior. It is evident that these computed values, $C_k/m(0)$ and T_k, are very similar to the experimental pattern in eq II (cf. Table II and Figure 4c) and we want to emphasize that the experimental results at least do not contradict the scheme.

Undoubtedly, Scheme I displays only one of the possible mechanisms and it appears from preliminary computational experiments that similar versions of energy cascading events will lead to transient profiles which also fit the experimental data qualitatively.

We must admit, however, that the evaluation of numerically resolvable exponentials together with their correlation to excited-state entities must be considered to be only a modest attempt for the description of the excited-state dynamics of p-N-VCz. Thus, the incorporation of novel phantom traps Tr_1 and Tr_2 and their interrelation to the excimer states E_1 and E_2 is only an approach which might account for a series of energy cascading events on the nanosecond time scale, provided that energy migration will have no interfering effect upon the number of resolvable exponentials in the long-time limit of these processes. Under such circumstances we might expect trap–monomer conversion (k_{1M}), trap–trap interrelation (k_{12}, k_{21}), rotational sampling (k_{13}, k_{23}), and excimer dissociation (k_{31}, k_{32}) to become the rate-determining steps.

Nevertheless, we must take into account that energy migration and trapping in p-N-VCz are ultrafast processes which—in accordance with the results of recent model calculations[41-43]—must be assumed to be highly nondiffusive in nature. Therefore, it is certainly not appropriate to use exponential trapping rate constants (k_{M1}, k_{M2}, k_{M5}), particularly for the description of monomer deactivation and trap population in the transient picosecond regime. Recent theoretical studies by Fredrickson and Frank[66] on polyaromatic, unidimensional model chains have shown the rather problematic character of this treatment of multiexponential data analysis.

As to p-N-VCz in dilute solution, the morphology of its random coil is presumably more complex, which means that it cannot be modeled through a quasi-one-dimensional chain. Due to the nonuniform distribution of monomeric carbazole chromophores and dimeric traps, p-N-VCz represents an anisotropic medium which induces higher dimensional contributions of interchromophoric, intrachain coupling. In addition, the existence of two excimer states E_1 and E_2 in p-N-VCz, as well as one or the other presumable trap species, will lead to further complications in the course of excited-state transport. Finally, the dissociative behavior of the sandwich excimer E_2, as well as the existence of reversible pathways in energy trapping, must result in a serious perturbation inasmuch as the downchain excitation energy transfer cannot be terminated quantitatively.

In any case, all these kinetic complications, which must proceed in p-N-VCz, are expected to complicate the profiles of both the monomer deactivation and the trap population, though exact analytical solutions for the respective response functions of energy donor and energy acceptor

are not available so far. Thus, as a first approach to these problems (a) the development of iterative reconvolution routines based on semiempirical, nonexponential trial functions and (b) the improvement of time resolution in general might lead to considerable progress in transient data analysis of fluorescent polymeric systems.

Acknowledgment. This work was supported by the Fonds zur Förderung der Wissenschaftlichen Forschung, Wien, Austria (Grant No. 4309), which is gratefully acknowledged. We appreciate the generous help of Dr. G. Gleixner, Institute of Physical Chemistry, University of Vienna, concerning the problems of polymer purification by GPC techniques. H.F.K. thanks Prof. Dr. W. Klöpffer, Battelle Institute, Frankfurt/M, FRG, for reading the manuscript and for stimulating discussion.

Registry No. *p-N*-VCz (homopolymer), 25067-59-8.

Supplementary Material Available: Mathematical treatment of the proposed scheme (10 pages). Ordering information is given on any current masthead page.

References and Notes

(1) Ghiggino, K. P.; Wright, R. D.; Phillips, D. *J. Polym. Sci., Polym. Phys. Ed.* **1978**, *16*, 1499.
(2) Rumbles, G. In "Photophysics of Synthetic Polymers"; Phillips, D., Roberts, A. J., Eds.; The Royal Institution; Science Reviews Ltd.: Northwood, England, 1982, p.5
(3) Phillips, D.; Roberts, A. J.; Rumbles, G.; Soutar, I. *Macromolecules* **1983**, *16*, 1198.
(4) Ghiggino, K. P.; Wright, R. D.; Phillips, D. *Chem. Phys. Lett.* **1978**, *53*, 552.
(5) Phillips, D.; Roberts, A. J.; Soutar, I. *Polymer* **1981**, *22*, 427.
(6) Gupta, A.; Liang, R.; Mocanin, J.; Kliger, D.; Goldenbeck, R.; Horwitz, J.; Miskowski, V. M. *Eur. Polym. J.* **1981**, *17*, 485.
(7) Demeyer, K.; Van der Auweraer, M.; Aerts, L.; De Schryver, F. C. *J. Chim. Phys. Phys.-Chim. Biol.* **1980**, *77*, 493.
(8) De Schryver, F. C.; Demeyer, K.; Van der Auweraer, M.; Quanten, E. *Ann. N.Y. Acad. Sci.* **1981**, *366*, 93.
(9) Holden, D. A.; Ren, X. X.; Guillet, J. E. *Macromolecules*, submitted for publication.
(10) Roberts, A. J.; O'Connor, D. V.; Phillips, D. *Ann. N.Y. Acad. Sci.* **1981**, *366*, 109.
(11) Phillips, D.; Roberts, A. J.; Soutar, I. *J. Polym. Sci., Polym. Phys. Ed.* **1980**, *18*, 2401.
(12) Phillips, D.; Roberts, A. J.; Soutar, I. *J. Polym. Sci., Polym. Phys. Ed.* **1982**, *20*, 411.
(13) Phillips, D.; Roberts, A. J.; Soutar, I. *Polymer* **1981**, *22*, 293.
(14) Ito, S.; Yamamoto, M.; Nishijima, Y. *Polym. J.* **1981**, *13*, 791.
(15) Holden, D. A.; Guillet, J. E. *Macromolecules* **1980**, *13*, 289.
(16) Holden, D. A.; Wang, P. Y.-K.; Guillet, J. E. *Macromolecules* **1980**, *13*, 295.
(17) Merle-Aubry, L.; Holden, D. A.; Merle, Y.; Guillet, J. E. *Macromolecules* **1980**, *13*, 1138.
(18) Holden, D. A.; Guillet, J. E. *Macromolecules* **1982**, *15*, 1475.
(19) Birks, J. B.; Dyson, D. J.; Munro, I. H. *Proc. R. Soc. London, Ser. A* **1963**, *275*, 575.
(20) Birks, J. B. "Photophysics of Aromatic Molecules"; Wiley-Interscience: New York, 1970; Chapter 7.
(21) Klöpffer, W. In "Organic Molecular Photophysics"; Birks, J. B., Ed.; Wiley: New York, 1973; Vol. 1, p 357.
(22) Klöpffer, W.; Liptay, W. *Z. Naturforsch., A* **1970**, *25a*, 1091.
(23) Klöpffer, W. *Chem. Phys. Lett.* **1969**, *4*, 193.
(24) Itagaki, H.; Okamoto, A.; Horie, K.; Mita, I. *Eur. Polym. J.* **1982**, *18*, 885.
(25) Itagaki, H.; Obukata, N.; Okamoto, A.; Horie, K.; Mita, I. *J. Am. Chem. Soc.* **1982**, *104*, 4469.
(26) Todesco, R.; Gelan, J.; Martens, H.; Put, J.; De Schryver, F. C. *J. Am. Chem. Soc.* **1981**, *103*, 7304.
(27) Goldenberg, M.; Emert, J.; Morawetz, H. *J. Am. Chem. Soc.* **1978**, *100*, 7171.
(28) Ng, D.; Guillet, J. E. *Macromolecules* **1981**, *14*, 405.
(29) Johnson, G. E. *J. Chem. Phys.* **1975**, *62*, 4697.
(30) Hoyle, C. E.; Nemzek, T. L.; Mar, A.; Guillet, J. E. *Macromolecules* **1978**, *11*, 429.
(31) Ghiggino, K. P.; Archibald, D. A.; Thistlethwaite, P. J. *J. Polym. Sci., Polym. Lett.* Ed. **1980**, *18*, 673.
(32) De Schryver, F. C.; Vandendriesche, J.; Toppet, S.; Demeyer, K.; Boens, N. *Macromolecules* **1982**, *15*, 406.
(33) Evers, F.; Kobs, K.; Memming, R.; Terrell, D. R. *J. Am. Chem. Soc.* **1983**, *105*, 5988.
(34) Itaya, A.; Okamoto, K.; Kusabayashi, S. *Bull. Chem. Soc. Jpn.* **1976**, *49*, 2082.
(35) Ghiggino, K. P.; Wright, R. D.; Phillips, D. *Eur. Polym. J.* **1978**, *14*, 567.
(36) See, for example: Knox, R. S. In "Bioenergetics of Photosynthesis"; Govindjee, Ed.; Academic Press: New York, 1975; p 183.
(37) See, for example: Klöpffer, W. In "Electronic Properties of Polymers"; Mort, J., Pfister, G., Eds., Wiley: New York, 1982.
(38) Klöpffer, W. *J. Chem. Phys.* **1969**, *50*, 2337.
(39) Roberts, A. J.; Cureton, C. G.; Phillips, D. *Chem. Phys. Lett.* **1980**, *72*, 554.
(40) Roberts, A. J.; Phillips, D. *Macromolecules* **1982**, *15*, 678.
(41) Fredrickson, G. H.; Frank, C. W. *Macromolecules* **1983**, *16*, 1198.
(42) Fredrickson, G. H.; Andersen, H. C.; Frank, C. W. *Macromolecules* **1983**, *16*, 1456.
(43) Fredrickson, G. H.; Andersen, H. C.; Frank, C. W. *J. Chem. Phys.* **1983**, *79*, 3572.
(44) Houben, J. L.; Natucci, B.; Solaro, R.; Colella, O.; Chiellini, E.; Ledwith, A. *Polymer* **1978**, *19*, 811.
(45) Chapoy, L. L.; Biddle, D. *J. Polym. Sci., Polym. Lett. Ed.* **1983**, 621.
(46) Roberts, A. J.; Phillips, D.; Abdul-Rasoul, F. A. M.; Ledwith, A. *J. Chem. Soc., Faraday Trans. 1* **1981**, *77*, 2725.
(47) Knutson, J. R.; Walbridge, D. G.; Davenport, L.; Pritt, M. D.; Brand, L. In "Deconvolution–Reconvolution"; Bouchy, M., Ed.; ENSIC-INPL: Nancy, France, 1982.
(48) Heisel, F.; Miehe, J. A. *J. Chem. Phys.* **1982**, *77*, 2558.
(49) Sipp, B.; Voltz, R. *J. Chem. Phys.* **1983**, *79*, 434.
(50) Itagaki, H.; Horie, K.; Mita, I. *Macromolecules* **1983**, *16*, 1395.
(51) Simionescu, C. I.; Percec, V.; Natansohn, A. *Polymer* **1980**, *21*, 417.
(52) Easter, J. H.; DeToma, R. P.; Brand, L. *Biophys. J.* **1976**, *16*, 571.
(53) Grinvald, A.; Steinberg, I. Z. *Anal. Biochem.* **1974**, *59*, 583.
(54) O'Connor, D. V.; Ware, W. R.; André, J. C. *J. Phys. Chem.* **1979**, *83*, 1333.
(55) Marquardt, D. W. *J. Soc. Ind. Appl. Math.* **1963**, *11*, 431.
(56) See, for example: Demas, J. N. "Excited State Lifetime Measurements"; Academic Press: New York, 1983; Chapter 5.
(57) Wahl, P.; Auchet, J. C.; Doncel, B. *Rev. Sci. Instrum.* **1974**, *45*, 28.
(58) Birch, D. J. S.; Imhof, R. E. *Chem. Phys. Lett.* **1982**, *88*, 243.
(59) Ware, W. R.; Pratinidhi, M.; Bauer, R. K. *Rev. Sci. Instrum.* **1983**, *54*, 1148.
(60) Johnson, G. E. *J. Phys. Chem.* **1974**, *78*, 1512.
(61) Webber, S. E.; Avots-Avotins, P. E.; Deumié, M. *Macromolecules* **1981**, *14*, 105.
(62) Johnson, G. E. *J. Chem. Phys.* **1974**, *61*, 3002.
(63) Berlman, I. B. "Fluorescence Spectra of Aromatic Molecules"; Academic Press: New York, 1971.
(64) Tagawa, S.; Washio, M.; Tabata, Y. *Chem. Phys. Lett.* **1979**, *68*, 276.
(65) Note: (a) The fixed quantity k_M is evaluated from a simple lifetime measurement of an undisturbed carbazole chromophore. Both for the copolymer in Figure 1, curve d, and for *N*-ethylcarbazole in benzene, we found T_M = 12 ns, corresponding to $1/T_M \cong 0.83E + 0.8$. k_1 and k_2 of the dimeric traps Tr_1 and Tr_2 are assumed to be not markedly different from a monomeric carbazole group in this evaluation. (b) k_3, reciprocal effective lifetime of E_2 in the absence of dissociation, estimated from the low-temperature lifetime of the respective carbazole double molecules,[60] according to $1/k_3 \cong 45$ ns. (c) Experimental quantity, T_5; see also ref 46.
(66) Fredrickson, G. H.; Frank, C. W. *Macromolecules* **1983**, *16*, 572.